

Bipolar-growth multi-wing attractors and diverse coexisting attractors in a new memristive chaotic system

Wang-Peng Huang(黄旺鹏) and Qiang Lai(赖强)
Citation: Chin. Phys. B, 2023, 32 (**10**): 100504. DOI: 10.1088/1674-1056/ace1d9
Journal homepage: http://cpb.iphy.ac.cn; http://iopscience.iop.org/cpb

What follows is a list of articles you may be interested in

Critical dispersion of chirped fiber Bragg grating for eliminating time delay signature of distributed feedback laser chaos

Da-Ming Wang(王大铭), Yi-Hang Lei(雷一航), Peng-Fei Shi(史鹏飞), and Zhuang-Ai Li(李壮爱)
Chin. Phys. B, 2023, 32 (**9**): 090505. DOI: 10.1088/1674-1056/acddce

A novel fractional-order hyperchaotic complex system and its synchronization

Mengxin Jin(金孟鑫), Kehui Sun(孙克辉), and Shaobo He(贺少波)
Chin. Phys. B, 2023, 32 (**6**): 060501. DOI: 10.1088/1674-1056/acc0f6

Unstable periodic orbits analysis in the Qi system

Lian Jia(贾莲), Chengwei Dong(董成伟), Hantao Li(李瀚涛), and Xiaohong Sui(眭晓红)
Chin. Phys. B, 2023, 32 (**4**): 040502. DOI: 10.1088/1674-1056/aca9c3

A color image encryption algorithm based on hyperchaotic map and DNA mutation

Xinyu Gao(高昕瑜), Bo Sun(孙博), Yinghong Cao(曹颖鸿), Santo Banerjee, and Jun Mou(牟俊)
Chin. Phys. B, 2023, 32 (**3**): 030501. DOI: 10.1088/1674-1056/ac8cdf

Lossless embedding: A visually meaningful image encryption algorithm based on hyperchaos and compressive sensing

Xing-Yuan Wang(王兴元), Xiao-Li Wang(王晓丽), Lin Teng(滕琳), Dong-Hua Jiang(蒋东华), and Yongjin Xian(咸永锦)
Chin. Phys. B, 2023, 32 (**2**): 020503. DOI: 10.1088/1674-1056/aca149

Bipolar-growth multi-wing attractors and diverse coexisting attractors in a new memristive chaotic system

Wang-Peng Huang(黄旺鹏)[1] and Qiang Lai(赖强)[1,2,†]

[1] *School of Tian You, East China Jiaotong University, Nanchang* 330013, *China*
[2] *School of Electrical and Automation Engineering, East China Jiaotong University, Nanchang* 330013, *China*

(Received 18 May 2023; revised manuscript received 24 June 2023; accepted manuscript online 27 June 2023)

This article proposes a non-ideal flux-controlled memristor with a bisymmetric sawtooth piecewise function, and a new multi-wing memristive chaotic system (MMCS) based on the memristor is generated. Compared with other existing MMCSs, the most eye-catching point of the proposed MMCS is that the amplitude of the wing will enlarge towards the poles as the number of wings increases. Diverse coexisting attractors are numerically found in the MMCS, including chaos, quasi-period, and stable point. The circuits of the proposed memristor and MMCS are designed and the obtained results demonstrate their validity and reliability.

Keywords: chaos, memristive chaotic system, multi-wing attractors, coexisting attractors

PACS: 05.45.Ac **DOI:** 10.1088/1674-1056/ace1d9

1. Introduction

In 1963, Lorenz discovered the classic butterfly attractor and first proposed the concept of chaotic systems.[1] Many theories on chaotic systems have been established in the decades since then. Chaos has drawn much attention from various academics due to chaos behaving randomly and unpredictably. What is more, it had a lot of essential applications in image encryption, security, and other engineering fields.[2–8]

In the past few decades, researchers have been exploring the chaos that can produce complex dynamical behavior, and it is worth mentioning that multi-scroll attractors and coexisting attractors have become a hot topic in nonlinear research.[9–19] The state variable can go through multiple orbital states and jump randomly in different transitions for the multi-scroll attractors. The coexisting attractors can provide multiple optional steady states for the system to respond to different needs, so it is very meaningful to construct multi-scroll systems with abundant coexisting attractors. On the other hand, memristors are the fourth fundamental circuit component, reflecting the nonlinear relationship between current and voltage, expressed via a shrinking hysteresis loop.[20] Besides, the memristor has lower power consumption, smaller size, and memory characteristics, making it particularly useful for studying nonlinear science, especially chaos.[21–26] Thus, memristors are often added to chaotic systems as nonlinear terms to construct more complex dynamical behavior and more multi-scroll attractors.[27,28]

In recent years, much research has been done on the non-memristor-based multi-scroll chaotic systems, but the memristor-based chaotic systems have infinite scrolls, which are still rare.[29–33] Xia *et al.*[25] proposed two kinds of novel non-ideal voltage-controlled memristors. Adding these memristor models to a three-dimensional (3D) jerk system establishes a novel memristive multi-scroll hyperchaotic jerk system with $2N+2$-scroll and $2M+1$-scroll hyperchaotic attractors. Lai *et al.*[35] based on a simple 3D chaotic system, grid-scroll chaotic attractors were constructed by adding a flux-controlled non-volatile memristor. Yu *et al.*[36] designed a novel local active and non-volatile memristor and constructed a four-dimensional (4D) memristive Hopfield neural network with the memristor, which have controllable double-scroll attractors. Lai *et al.*[37] presented a new Hopfield neural network (HNN) that can generate multi-scroll attractors by utilizing a new memristor as a synapse in the HNN.

The above review of the MMCS shows that there are still two issues for further consideration. For one issue, although the number of scrolls in the MMCS has increased, the size of expanded scrolls is not changed. For another issue, the coexisting attractors of the MMCS mentioned above are not rich due to the coexisting attractors are homogeneous. Inspired by the above-mentioned considerations, we propose a bipolar-growth multi-wing memristive chaotic system (BMMCS), numerically drawing the phase planes with different parameters of BMMCS and analyzing the dynamic behavior of BMMCS by the bifurcation diagrams and Lyapunov exponents (LEs).

2. Chaotic system with a memristor model

2.1. System and memristor description

We obtained the following numerical simulation results through Matlab2018a. Setting the step size of phase planes,

†Corresponding author. E-mail: laiqiang87@126.com

© 2023 Chinese Physical Society and IOP Publishing Ltd

bifurcation diagrams and LEs to 0.01, 0.5, and 0.1.

Considering a simple chaotic system[38]

$$\begin{cases} \dot{x} = yz, \\ \dot{y} = z^2 - 1, \\ \dot{z} = -yz + x, \end{cases} \tag{1}$$

where x, y, z are different state variables. We propose a non-ideal flux-controlled memristor model. By coupling the memristor and adding a linear term to system (1), we can obtain BMMCS

$$\begin{cases} \dot{x} = yz, \\ \dot{y} = z^2 - 1, \\ \dot{z} = -ayz - W(\varphi)x - bz, \\ \dot{\varphi} = x - \varphi, \end{cases} \tag{2}$$

where a, b are positive parameters, φ is the internal state variable of the memristor. The memristor model can be expressed as

$$\begin{cases} i = W(\varphi)v, \\ \dot{\varphi} = v - \varphi, \end{cases} \tag{3}$$

with the current i, voltage v, flux φ. The memductance function $W(\varphi)$ is described as

$$W(\varphi) = \frac{2}{k}|\varphi| - 2N - 1 + \sum_{i=0}^{N} [\mathrm{sgn}(\varphi + ki) - \mathrm{sgn}(\varphi - ki)], \tag{4}$$

where $k > 0$ and $N = 0, 1, 2 \ldots$. Let $k = 1$ and $N = 0, 1$, we obtain

$$\begin{cases} W(\varphi) = 2|\varphi| - 1, (N = 0), \\ W(\varphi) = 2|\varphi| + \mathrm{sgn}(\varphi + 1) - \mathrm{sgn}(\varphi - 1) - 3, \ (N = 1), \end{cases} \tag{5}$$

and the curves of Eq. (5) are displayed in Fig. 1. We numerically calculate the relationship between voltage and current, the input voltage $v = v_q \sin(2\pi f t)$ with voltage amplitude v_q and power frequency f. Let $v_q = 5$ V, $k = 5$, $N = 1$, and f respectively set as 0.1 Hz, 1 Hz, 10 Hz, then keep $f = 1$ Hz, set $v_q = 5$ V, 8 V, 10 V, the results are presented in Fig. 2.

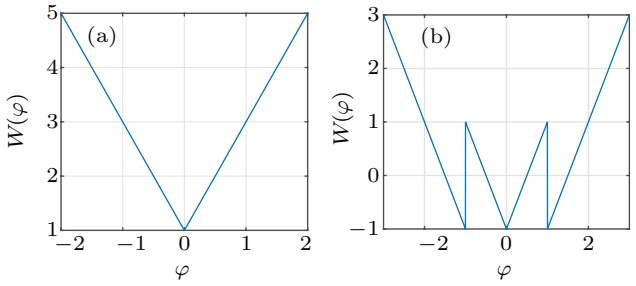


Fig. 1. Function $W(\varphi)$ for (a) $k = 1$, $N = 0$; (b) $k = 1$, $N = 1$.

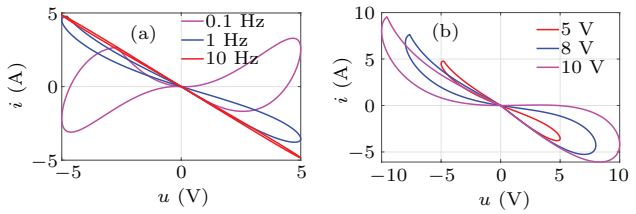


Fig. 2. Pinched hysteresis loops of the memristor for (a) frequency $f = 0.1$ Hz, 1 Hz, 10 Hz; (b) amplitude $v_q = 5$ V, 8 V, 10 V.

In addition, we design the equivalent circuit model of the memristor as shown in Fig. 3. One selects the IN4148 diode, operational amplifier TL082 is powered by ±15 V-dc, and the multiplier AD633JN gains 0.1. Let $C_1 = 100$ nF, $R_0 = 100$ kΩ, $R_1 = 10$ MΩ, $R_2 = 10$ MΩ, the memristor circuit is powered by sinusoidal voltage source $V_p \sin(2\pi F t)$, which V_p is voltage amplitude, and F is power frequency. Selecting $V_p = 5$ V, $k = 5$, $N = 1$, and let $F = 0.1$ Hz, 10 Hz, the relationship between voltage and current is displayed in Fig. 4. The numerical simulation and circuit experiment both show that the flux-controlled memristor can exhibit pinched hysteresis loops that pinched at the origin. The lobe area decreases with the increase in frequency.

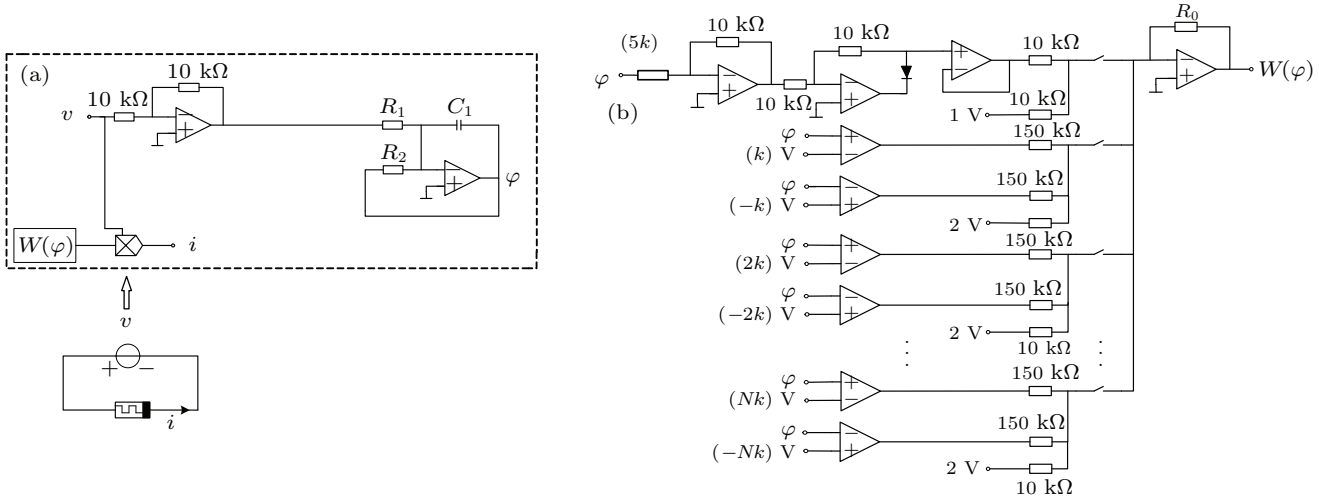


Fig. 3. (a) Equivalent memristor circuit, (b) detailed $W(\varphi)$.

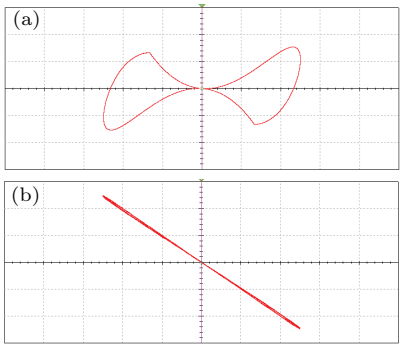


Fig. 4. The relationship between voltage and current of the memristor for: (a) $f = 0.1$ Hz, (b) $f = 10$ Hz.

2.2. Equilibrium points and stability analysis

Suppose $S(\tilde{x}, \tilde{y}, \tilde{z}, \tilde{\varphi})$ is an equilibrium point of BBMCS, then

$$\begin{cases} \tilde{y}\tilde{z} = 0, \\ \tilde{z}^2 - 1 = 0, \\ -a\tilde{y}\tilde{z} - W(\tilde{\varphi})\tilde{x} - b\tilde{z} = 0, \\ \tilde{x} - \tilde{\varphi} = 0. \end{cases} \tag{6}$$

By solving Eq. (6), one has $\tilde{x} = \tilde{\varphi}$, $W(\tilde{\varphi})\tilde{\varphi} = \pm b$, $\tilde{y} = 0$, and $\tilde{z} = \pm 1$. Linearizing BBMCS at $S(\tilde{\varphi}, 0, \pm 1, \tilde{\varphi})$, the Jacobian matrix is obtained as

$$\boldsymbol{J} = \begin{pmatrix} 0 & \pm 1 & 0 & 0 \\ 0 & 0 & \pm 2 & 0 \\ -W(\tilde{\varphi}) & \mp a & -b & -W'(\tilde{\varphi})\tilde{\varphi} \\ 1 & 0 & 0 & -1 \end{pmatrix}.$$

By calculating $|\lambda \boldsymbol{I} - \boldsymbol{J}| = 0$, we can get the characteristic equation is

$$\lambda^4 + m_1\lambda^3 + m_2\lambda^2 + m_3\lambda + m_4 = 0, \tag{7}$$

where $m_1 = b + 1$, $m_2 = 2a + b$, $m_3 = 2a + 2W(\tilde{\varphi})$, $m_4 = 2W(\tilde{\varphi}) + 2W'(\tilde{\varphi})\tilde{\varphi}$. For the parameters $a = 0.74$, $b = 2.8$, $k = 5$, $N = 1$, BBMCS can produce 10 equilibrium points. Taking them into Eq. (7), their corresponding eigenvalues and equilibrium point types are shown in Table 1.

Table 1. The eigenvalues and types of equilibrium points.

Equilibrium points	Eigenvalues	Types
(–5,0,±1,–5)	$\lambda_1 = -10.9779, \lambda_2 = 9.0769,$	unstable index-1
(5,0,±1,5)	$\lambda_{3,4} = -0.9495 \pm 9.9707\mathrm{i}$	saddle-focus point
(–8.34,0,1,–8.34)	$\lambda_{1,2} = -2.2081 \pm 0.9168\mathrm{i},$	unstable index-2
(8.34,0,–1,8.34)	$\lambda_{3,4} = 0.3081 \pm 1.0908\mathrm{i}$	saddle-focus point
(–6.41,0,–1,–6.41)	$\lambda_{1,2} = -2.1395 \pm 0.9935\mathrm{i},$	unstable index-2
(6.41,0,1,6.41)	$\lambda_{3,4} = 0.2395 \pm 0.8411\mathrm{i}$	saddle-focus point
(–4.18,0,1,–4.18)	$\lambda_{1,2} = -2.0570 \pm 0.5547\mathrm{i},$	unstable index-2
(4.18,0,–1,4.18)	$\lambda_{3,4} = 0.1570 \pm 1.0041\mathrm{i}$	saddle-focus point

Table 2. The relationship between $\tilde{\varphi}_m$ and BF_n.

The range of n	$\tilde{\varphi}_m$	BF_n
$n < 0$	$(\tilde{\varphi}_{2n-1}, \tilde{\varphi}_{2n})$	BF_n
	⋮	⋮
	$(\tilde{\varphi}_{-5}, \tilde{\varphi}_{-4})$	BF_{-2}
	$(\tilde{\varphi}_{-3}, \tilde{\varphi}_{-2})$	BF_{-1}
$n = 0$	$(\tilde{\varphi}_{-1}, \tilde{\varphi}_{1})$	BF_0
$n > 0$	$(\tilde{\varphi}_{2}, \tilde{\varphi}_{3})$	BF_1
	$(\tilde{\varphi}_{4}, \tilde{\varphi}_{5})$	BF_2
	⋮	⋮
	$(\tilde{\varphi}_{2n}, \tilde{\varphi}_{2n+1})$	BF_n

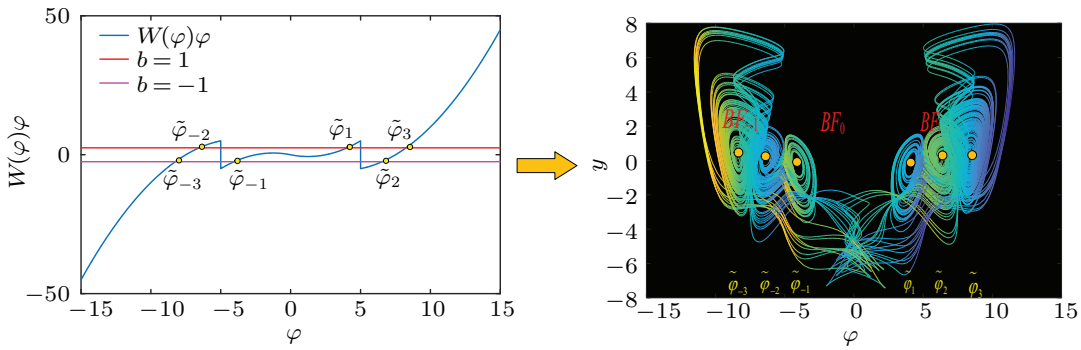


Fig. 5. The corresponding relationship between the BMMCS with a 6-wing attractor and $\tilde{\varphi}_m$.

Here $\tilde{\varphi}_m$, BF_n ($|m| = 1, 2, 3, \ldots$, $|n| = 0, 1, 2, \ldots$) respectively represent the unstable index-2 saddle-focus points on the φ-axis and the expanded 2-wing attractors, the relationship between $\tilde{\varphi}_m$ and BF_n is described in Table 2, and their corresponding phase plane is shown in Fig. 5. It is obvious that the $\tilde{\varphi}$ of BF_0 is bipolar, and the others are unipolar. Hence BF_0 differs in shape from BF_n ($n \neq 0$). Let $N = 3$, $d_{|n|}$ is the distance of the two equilibrium points of BF_n on the φ-axis, and it can be seen that $d_{|n|}$ is smaller as $|n|$ increase from Fig. 6.

If $d_{|n|}$ is too small, BF_n will not appear. And we can increase b to broaden the distance so that one can obtain more BF_n as N increases, thus let $b = 6$, $N = 7$, the phase plane is displayed in Fig. 7. Moreover, we find that with the increase of $|n|$, the amplitude of BF_n becomes larger. So it can generate more BF_n with different amplitude ranges by controlling N and b. Meanwhile, figure 8 displays more phase planes of

BBMCS with $N = 0, 3$.

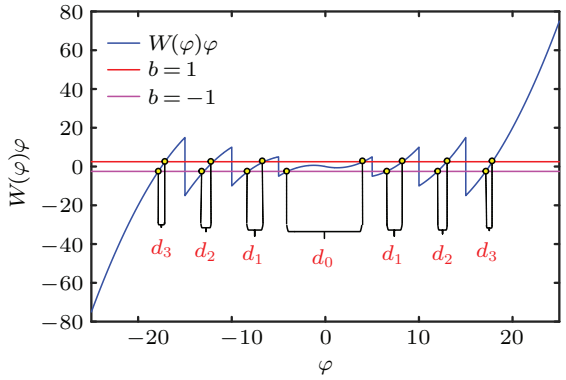


Fig. 6. The $d_{|n|}$ with $W(\varphi)\varphi = \pm 1$.

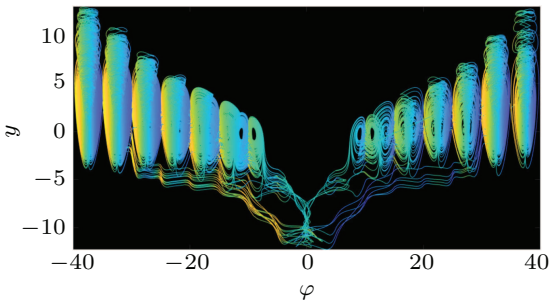


Fig. 7. BMMCS with a 26-wing attractor.

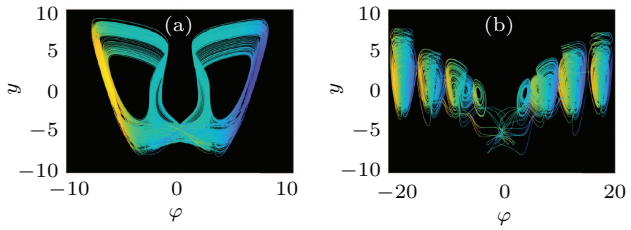


Fig. 8. BMMCS of the phase planes for (a) 2-wing attractor, (b) 14-wing attractor.

3. Dynamic analysis

3.1. Bifurcation diagrams and LEs

The parameters have a great influence on the dynamic behavior of chaotic systems, so we analyze the bifurcation diagrams and the LEs with a step size is 0.001.

Fixing $b = 2.8$, $k = 5$, $N = 2$, and $a \in [0.8,\ 1.4]$, the bifurcation diagram from Fig. 9(a) indicates that BBMCS has a 10-wing attractor. The LEs from Fig. 9(b) show that BBMCS has experienced chaos, quasi-period, and stable point. $a \in [0.8,\ 1.32)$ with a positive LE indicates that BBMCS is chaos. BBMCS with $a \in [1.32,\ 1.34]$ is quasi-period due to the first two LEs are zero. And all LEs less than zero shows that BBMCS is a stable point when $a \in (1.34,\ 1.4]$. Accordingly, setting $a = 1,\ 1.21,\ 1.34,\ 1.4$, the phase planes of BBMCS are shown in Fig. 10. It should be noted that the multi-wing attractor may break,[39] especially $a \in [1.1,\ 1.25]$, and we can find a 10-wing attractor and a 3-wing attractor from Figs. 10(a) and 10(b), respectively.

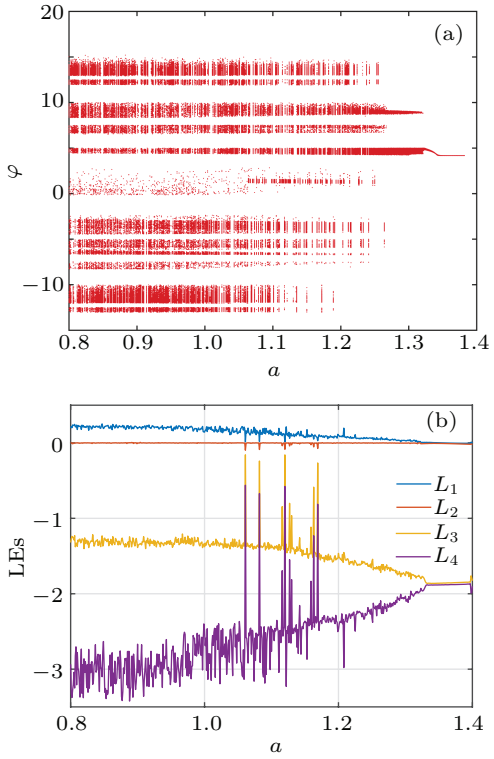


Fig. 9. (a) The bifurcation diagram about φ, (b) the LEs of the coexisting attractors with $N = 2$.

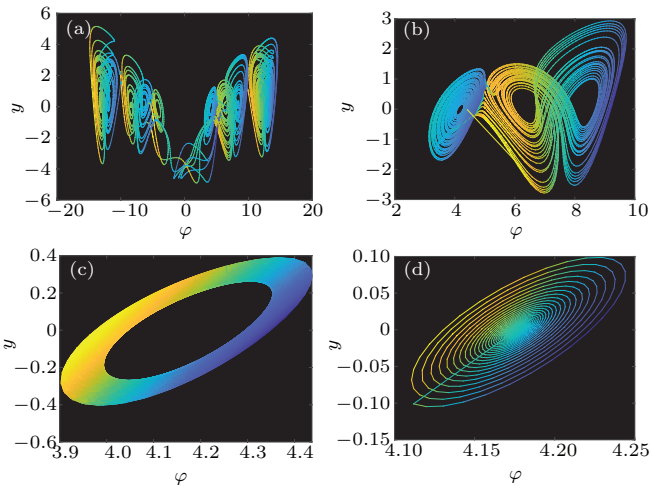


Fig. 10. The phase planes of BBMCS for (a) the multi-wing attractor with $a = 1$, (b) the broken chaotic attractor with $a = 1.21$, (c) the quasi-period with $a = 1.34$, (d) the stable point with $a = 1.4$.

3.2. Coexisting attractors

Adjusting $a = 1.8$, $b = 3$, $k = 6$, $N = 2$, and initial conditions set as $(x(0), 1, 1, 1)$, $x(0) \in [-20,\ 20]$, the bifurcation diagram of φ and the LEs are displayed in Fig. 11. From Fig. 11(a), it is obvious that BBMCS has coexisting attractors. And figure 11(b) shows that BBMCS has chaos, stable point, and quasi-period. Accordingly, let $x(0) = 0,\ \pm 5,\ \pm 10,\ \pm 15$, the phase planes are shown in Fig. 12. One can observe that the multi-wing attractor breaks up, BF_0 of BBMCS breaks up into a quasi-period and two stable points, the others break up into single BF_n.

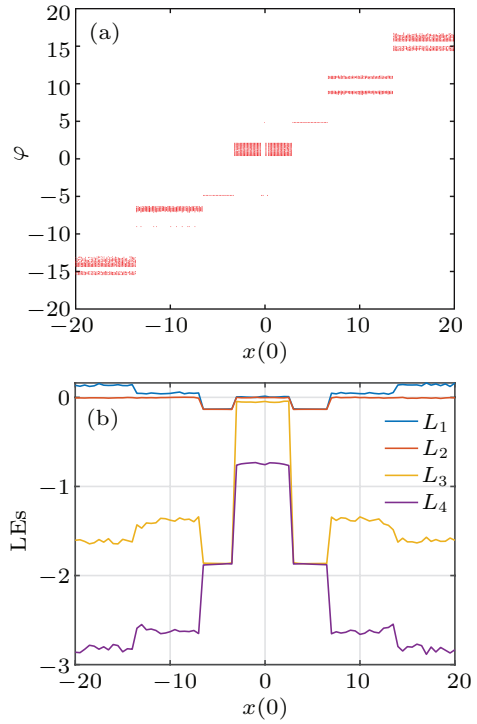


Fig. 11. (a) The bifurcation diagram of φ, (b) the LEs of the coexisting attractors with $N = 2$.

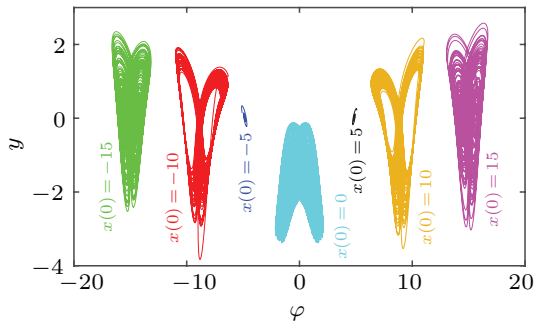


Fig. 12. The phase planes of the coexisting attractors with $N = 2$.

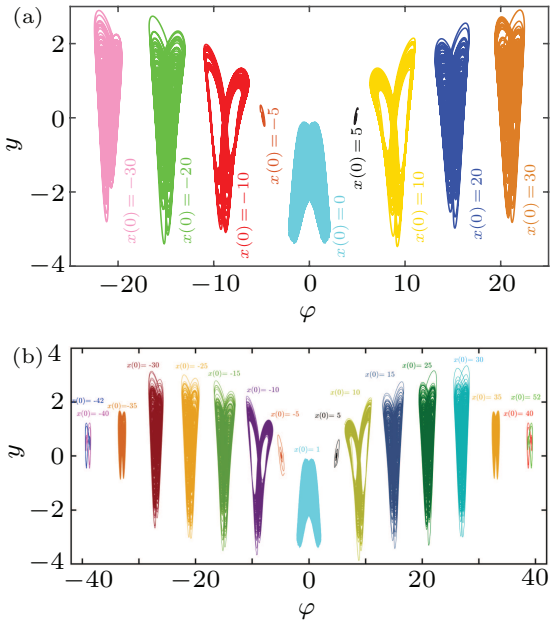


Fig. 13. The phase planes of the coexisting attractors for (a) $N = 3$ and (b) $N = 6$.

However, if $x(0)$ is less than -20 or greater than 20, the number of BF_n no longer increases with this parameter. It is found that N controls the number of the coexisting attractors, so set $N = 3, 6$, BBMCS can break up into 9 and 15 attractors. Correspondingly, the phase planes for the coexisting attractors can be obtained and shown in Fig. 13. From Fig. 13(b), it is worth noting that as $|n|$ increases, BF_n offset to the poles along the φ-axis. Meanwhile, the amplitude of BF_n also enlarges at $\varphi \in [-33, -7] \cup [7, 33]$. What is more, $d_{|n|}$ becomes smaller with $|n|$ increase, resulting in the coexisting attractors that begin to transform into the period as n increase at $\varphi \in [-52, -33] \cup [33, 52]$. Accordingly, let $x(0) \in [-50, 50]$, the bifurcation diagram about y and the LEs are displayed in Fig. 14.

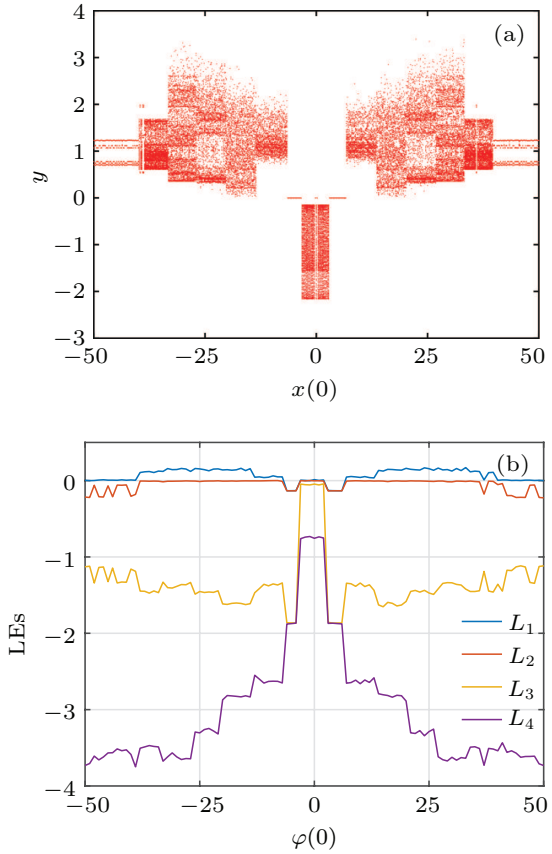


Fig. 14. (a) The bifurcation diagram about y and (b) the LEs of the coexisting attractors with $N = 6$.

We further studied the impact of tiny d_n on the formation of the multi-wing attractors. Let $a = 1$, $b = 0.8$, $k = 5$, $N = 2$, set $x(0) = \pm 0.5, \pm 10, \pm 15$. From Fig. 15(a), the phase planes show that the multi-wing attractor breaks up into periodic attractors. From Fig. 15(b), the bifurcation diagram about φ indicates that BBMCS is always in a periodic state under these parameters at $x(0) \in [-20, 20]$. Besides, with $|n|$ increase, the periodic attractors offset to the poles on the w axis as well as the positive on the y axis, and figure 16 shows 2 and 10 periodic attractors with $N = 0, 4$ in the phase planes.

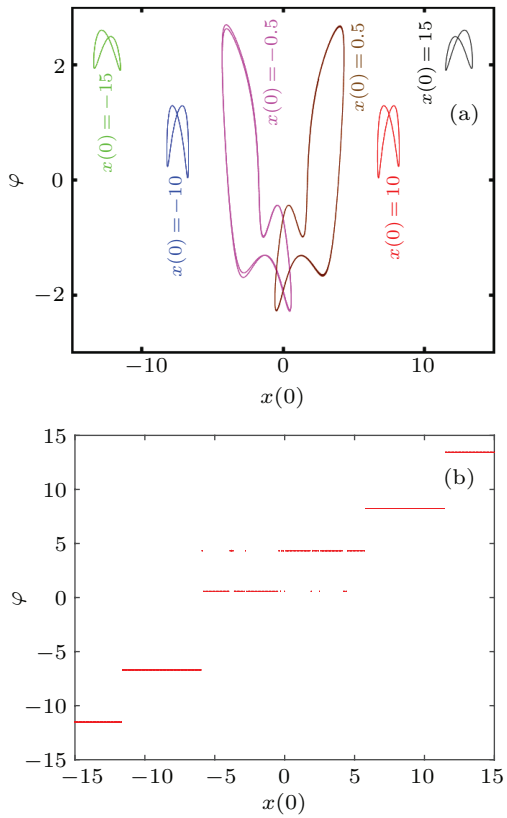


Fig. 15. Coexisting attractors with $N = 2$: (a) the phase plane on φ–y axis, (b) the bifurcation diagram about φ.

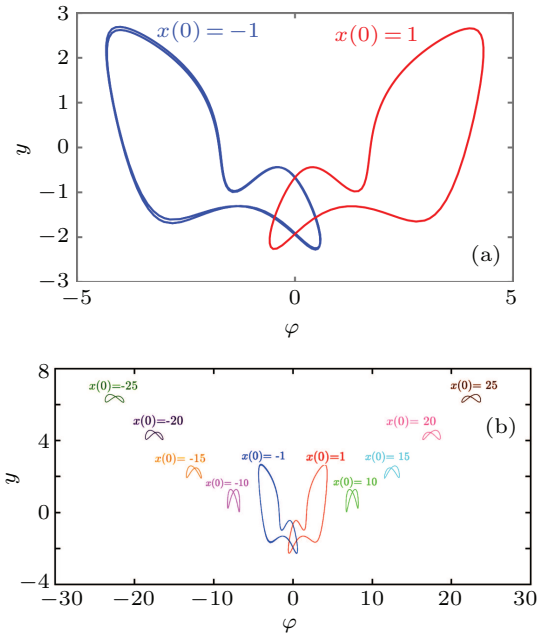


Fig. 16. The phase planes of the coexisting attractors for: (a) $N = 0$, (b) $N = 4$.

4. Circuit implementation

We designed the circuit with operational amplifiers TL082, switching diode 1N4148, multiplier AD633JN, and so on, as shown in Fig. 17. The powered voltages of operational amplifiers are ±15 V-dc, and the output gain of the multiplier is 0.1.

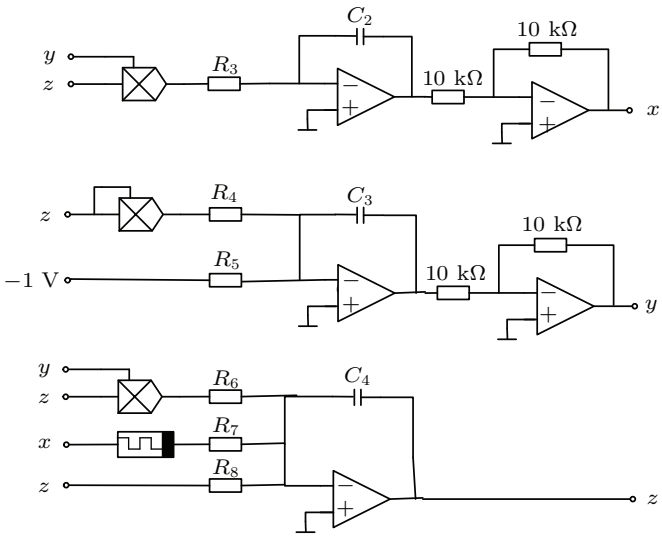


Fig. 17. The circuit diagram of BBMCS.

The state variables of BBMCS are compressed to ($2x$, $2y$, $2z$, 2φ), and BBMCS yield the following equations:

$$\begin{cases} \dot{v_x} = \dfrac{1}{RC_2}\left(\dfrac{R}{R_3}v_y v_z\right), \\ \dot{v_y} = \dfrac{1}{RC_3}\left(\dfrac{R}{R_4}v_z^2 - \dfrac{R}{R_5}\right), \\ \dot{v_z} = \dfrac{1}{RC_4}\left(-\dfrac{R}{R_6}v_y v_z - \dfrac{R}{R_7}W(2v_\varphi)v_x - \dfrac{R}{R_8}v_z\right), \\ \dot{v_\varphi} = \dfrac{1}{RC_1}\left(\dfrac{R}{R_1}v_x - \dfrac{R}{R_2}v_\varphi\right), \end{cases} \tag{8}$$

where R is a reference resistor, v_x, v_y, v_z, v_φ are the terminal voltages of C_1, C_2, C_3, C_4, and separately correspond to the state variables x, y, z, φ of BBMCS.

Setting $R = 10$ kΩ, $C_1 = C_2 = C_3 = C_4 = 100$ nF, and BBMCS with parameters $a = 0.74$, $b = 2.7$, $k = 5$, $N = 1$, 2. The circuit parameters can be obtain as $R_0 = R_2 = 10$ kΩ, $R_1 = 5$ kΩ, $R_3 = R_4 = 500$ Ω, $R_5 = 20$ kΩ, $R_6 = 680$ Ω, $R_7 = 1$ kΩ, $R_8 = 3.6$ kΩ. Figure 18 shows the experimental results with a 3-wing and 10-wing attractor.

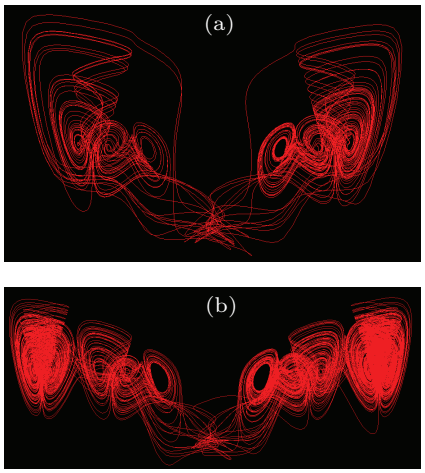


Fig. 18. The experimental results for (a) 6-wing attractor and (b) 10-wing attractor.

5. Conclusion

This paper proposed a non-ideal flux-controlled memristor with a bisymmetric sawtooth piecewise function. BMMCS was generated based on the memristor. It should be noted that BF_n can expand to the poles, and the amplitude of the wing will gradually enlarge. Another significant feature was that BBMCS had rich coexisting attractors including chaos, quasi-period, stable point. More interestingly, when the multi-wing attractors break up into periodic attractors, the periodic attractors will offset to the poles on the w axis as well as the positive on the y axis with $|n|$ increase. We designed the circuit of BBMCS, and the experimental results showed the reliability of BMMCS. It is worth noting that the amplitude of the scroll enlarges as the number of scroll increase in MMCS. This kind of attractor has a more complex structure and richer dynamic behavior, it has more extensive application value in engineering, and there is still much room for further study on this type of system.

Acknowledgements

Project supported by the National Natural Science Foundation of China (Grant Nos. 62366014 and 61961019) and the Natural Science Foundation of Jiangxi Province, China (Grant No. 20232BAB202008).

References

[1] Lorenz E N 1963 *Journal of the Atmospheric Sciences* **20** 130
[2] Lai Q, Hu G, Erkan U and Toktas A 2023 *Expert Systems with Applications* **213** 118845
[3] Gao X, Sun B, Cao Y H, Banerjee S and Mou J 2023 *Chin. Phys. B* **32** 030501
[4] Lai Q, Yang L and Liu Y 2022 *Chaos, Solitons & Fractals* **165** 112781
[5] Ma M L, Xiaong K L, Li Z J and He S B 2023 *Chin. Phys. B* **32**
[6] Alamodi A O A, Sun K H, Ai W, Chen C and Peng D 2019 *Chin. Phys. B* **28** 020503
[7] Lai Q and Yang L 2022 *IEEE Transactions on Circuits and Systems II: Express Briefs* **70** 1625
[8] Peng Y X, Sun K H and He S B 2022 *Chin. Phys. B* **29** 030502
[9] Jia S H, Li Y X, Shi Q Y and Huang X 2022 *Chin. Phys. B* **31** 070505
[10] Sahoo S and Roy B K 2022 *Chaos, Solitons & Fractals* **164** 112598
[11] Wang M J, Deng Y, Liao X H, Li Z J, Ma M L and Zeng Y C 2019 *International Journal of Nonlinear Mechanics* **111** 149
[12] Lin Y, Zhou X F, Gong J H, Yu F and Huang Y Y 2022 *Front. Phys.* **10** 927991
[13] Lai Q, Wan Z Q and Kuate P D K 2023 *IEEE Transactions on Circuits and Systems I: Regular Papers* **70** 1324
[14] Cui L, Luo W H and Ou Q L 2021 *Chin. Phys. B* **30** 020501
[15] Wan Q Z, Li F, Chen S M and Yang Q 2023 *Chaos, Solitons & Fractals* **169** 113259
[16] Bao H, Ding R Y, Chen B, Xu Q and Bao B C 2023 *Chaos, Solitons & Fractals* **169** 113228
[17] Zhang L P, Liu Y, Wei Z C, Jiang H B, Lyu W P and Bi Q S 2022 *Chin. Phys. B* **31** 100503
[18] Ma M, Lu Y, Li Z, Sun Y and Wang C 2023 *Fractal Fract.* **7** 82
[19] Balaraman S, Kengne J, Fogue M S K and Rajagopal K 2023 *Chaos, Solitons & Fractals* **172** 113619
[20] Chua L 1971 *IEEE Transactions on Circuit Theory* **18** 507
[21] Yu F, Zhang Z, Shen H, Huang Y Y, Cai S and Du S C 2022 *Chin. Phys. B* **31** 020505
[22] Sun Q K, He S B, Sun K H and Wang H H 2022 *Chin. Phys. B* **31** 120501
[23] Ma M L, Xie X H, Yang Y, Li Z J and Sun Y C 2023 *Chin. Phys. B* **32** 058701
[24] Ma M L, Xiong K L, Li Z J and Sun Y C 2023 *Mathematics* **11** 375
[25] Xie W L, Wang C H and Lin H R 2021 *Nonlinear Dyn.* **104** 4523
[26] Jiao X D, Yuan M F, Tao J, Sun H, Sun Q L and Chen Z Q 2023 *Chin. Phys. B* **32** 010507
[27] Jin J and Cui L 2019 *Complexity* **2019** 4106398
[28] Li R H, Wang Z H and Dong E Z 2021 *Nonlinear Dyn.* **104** 4459
[29] Zhou L, Wang C H and Zhou L L 2018 *International Journal of Circuit Theory and Applications* **46** 84
[30] Zhang S, Zheng J H, Wang X P, Zeng Z G and He S B 2020 *Nonlinear Dyn.* **102** 2821
[31] Zhang S, Zheng J H,Wang X P and Zeng Z G 2021 *Chaos* **31** 011101
[32] Li R H, Wang Z H and Dong E Z 2021 *Nonlinear Dyn.* **104** 4459
[33] Li F D and Zeng J R 2016 *Energies* **16** 2494
[34] Xia X Z, Zeng Y C and Li Z J 2018 *Pramana* **91** 82
[35] Lai Q and Chen Z J 2023 *Chaos, Solitons & Fractals* **170** 113341
[36] Yu F, Kong X X, Mokbel A A M, Wei Yao and Cai S 2022 *IEEE Transactions on Circuits and Systems II: Express Briefs* **70** 326
[37] Lai Q, Wan Z Q, Zhang H and Chen G R 2022 *IEEE Transactions on Neural Networks and Learning Systems*
[38] Li C B and Sprott J C 2016 *Optik* **127** 10389
[39] Li C B and Sprott J C 2014 *Int. J. Bifurc. Chaos* **24** 1450131